Mon. Not. R. astr. Soc. (1985) **215,** 517–536

The dynamical state of groups of galaxies

Joshua Barnes *Institute for Advanced Study, Princeton, NJ 08540, USA*

Accepted 1985 February 26. Received 1985 February 22; in original form 1985 January 3

Summary. Groups are likely sites for interaction and merging between galaxies, and may evolve significantly in a fraction of a Hubble time. This paper presents a series of *N*-body experiments modelling the evolution of groups of 5 to 10 galaxies with massive dark haloes, starting from a wide range of initial conditions. Galaxies with massive haloes 'stick together' on encounter and subsequently merge. Galaxy–galaxy and galaxy–background interactions extract orbital energy from the galaxies, which collect at the centre of the system. As a result, the dynamical mass and time-scales inferred using the galaxies significantly underestimate the true values for the system as a whole. Present-epoch groups, even those with apparently short ($\sim 0.1\ H_0^{-1}$) dynamical times, are probably relatively young objects which have only just collapsed; nevertheless, these groups have already undergone significant dynamical evolution, segregating the galaxies from the mass.

These results imply that (i) many group members are merger remnants, (ii) groups of galaxies evolve significantly on a dynamical time-scale, and (iii) the value of Ω estimated using the virial M/L ratios of groups is too low by a factor of ~ 3 or more.

1 Introduction

Galaxy clustering extends over a wide range of scales, from isolated binaries and satellite systems through rich Abell clusters and beyond to superclusters. Within this range, rich clusters have attracted the greatest interest. Observationally, they are spectacular objects, often containing unusually luminous galaxies, visible at great distances. Theoretically, they raise interesting questions concerning the effect of environment on galactic evolution; furthermore, the task of modelling rich clusters is fairly tractable, since typical velocity dispersions are much higher than those within galaxies.

Compact groups of galaxies, however, also raise interesting questions. Groups with interacting and apparently merging galaxies have been catalogued by Vorontsov-Vel'yaminov (1959) and Arp (1966). On the other hand, Hickson (1982) found comparatively little evidence for merging in a systematic catalogue of compact groups. Realistic dynamical theories for the evolution of small groups are difficult to construct, since few simplifying approximations are available. White

& Rees (1978) noted that the evolutionary time-scales for a lumpy self-gravitating system (e.g. a small group) are of the same order as the dynamical time. In their view, galaxies are able to maintain their identity as distinct objects within groups and clusters only because they formed from a gaseous component which was able to cool and collapse in potential wells provided by hierarchically clustering dark matter. The luminous part of a galaxy, having dissipated considerable binding energy, should be more resistant to merging and disruption than the associated dark halo.

N-body experiments relevant to groups and small clusters of galaxies have been done by Carnevali, Cavalere & Santangelo (1981) and Ishizawa *et al.* (1983). These simulations considered systems of 10 to 20 galaxies, each of which was modelled as a bound cluster of particles. Both studies found rapid and extensive merging between galaxies, generally confirming the theoretical predictions (Layzer 1977; White & Rees 1978). In interpreting these experiments, however, one must bear in mind that what is actually being simulated is probably the *dark* matter. Ishizawa *et al.* did identify the 10 per cent most tightly bound particles as a luminous component, but this technique is not completely satisfactory; as they note, the actual identify of this 10 per cent changes with time.

The paper describes an extensive series of *N*-body models of groups of galaxies, in which the evolution of distinct luminous and dark components is followed self-consistently. These simulations may be studied on several levels; the focus here is on comparing the overall properties of the models with observations. The outline is as follows: in Section 2 techniques and initial conditions are described, Section 3 gives results of the simulations, Section 4 makes the comparison with observations, and Section 5 discusses some implications of the results.

2 Techniques and initial conditions

The general approach taken here was to model each galaxy as a cloud of equal-mass particles; some were designated as luminous, while the rest represented dark matter. The luminous part will be referred to as the 'core', the dark part as the 'halo', while the term 'galaxy' will be used for the system as a whole. The number of stars in a galaxy far exceeds the capacity of any *N*-body code, so as usual each particle must represent many stars. This ploy introduces two problems. First, the models provide only a crude representation of actual galaxies. Second, two-body relaxation, which is insignificant in real galaxies, will occur in the models, unless a collisionless code is used. These simulations employed a direct summation code, in which all N^2 interparticle interactions were explicitly calculated, since a general method which could follow a wide range of scales was required. The equations of motion, derived from the softened 2-body potential

$$\phi_{ij}=\frac{-m_i m_j}{\sqrt{|\mathbf{r}_i-\mathbf{r}_j|^2+\max\ (\varepsilon_i,\ \varepsilon_j)^2}}, \tag{1}$$

(where ε_i is the softening length of the ith particle) were integrated with Dr Aarseth's NBODY1 code, adapted to use an array processor (Barnes 1984a); total binding energy was conserved to 0.01–0.1 per cent. Dark particles were typically given four times as much softening as luminous ones, suppressing relaxation in dark–dark and dark–luminous interactions. The smaller softening operating between luminous particles was necessary to follow the luminous matter on small scales; while relaxation occurred in this component, it is unlikely to have influenced the overall evolution of the models.

2.1 'HANDMADE' INITIAL CONDITIONS

To construct an *N*-body model of a single galaxy, a pair of King (1966) models were superimposed. The first model, with n_l particles, represents the luminous core; the second, with n_l+n_d, is

Table 1. Parameters for the handmade galaxy models. Subscripts 'l' and 'd' refer to the luminous core and dark halo components. The dimensionless central potentials of the King (1966) models used to set up the two components were $W_{cl}=7$, $W_{cd}=5$. The units used for ε and r_{hl} are the same as in Fig. 1.

Model	f_l	n_l	n_d	ϵ_l	ϵ_d	r_{hl}
g_1	0.1	30	270	0.025	0.1	0.04
g_2	0.2	30	120	0.05	0.2	0.08
g_3	0.2	20	80	0.05	0.2	0.08
g_4	0.4	30	45	0.1	0.2	0.16

the dark halo. Parameters for the two King models, for several choices of the ratio $f_l=n_l/(n_l+n_d)$ of luminous to total galactic mass, are listed in Table 1. The relative radii of the two models were proportional to their masses, so that they had approximately equal velocity dispersions. The first model was used to replace the n_l most bound particles of the second model; this insured that the core was self-bound (so that it could survive the stripping of its halo) and that the initial galaxy was close to dynamical equilibrium. The softening parameter adopted for the luminous particles, ε_l, was ~0.63 of the core half-mass radius; while this seriously perturbed the dynamics of the core, it prevented isolated cores from evolving significantly due to ordinary two-body relaxation. Softening had less effect on the halo dynamics, since the halo softening parameter, ε_d, was 0.25–0.5 of the

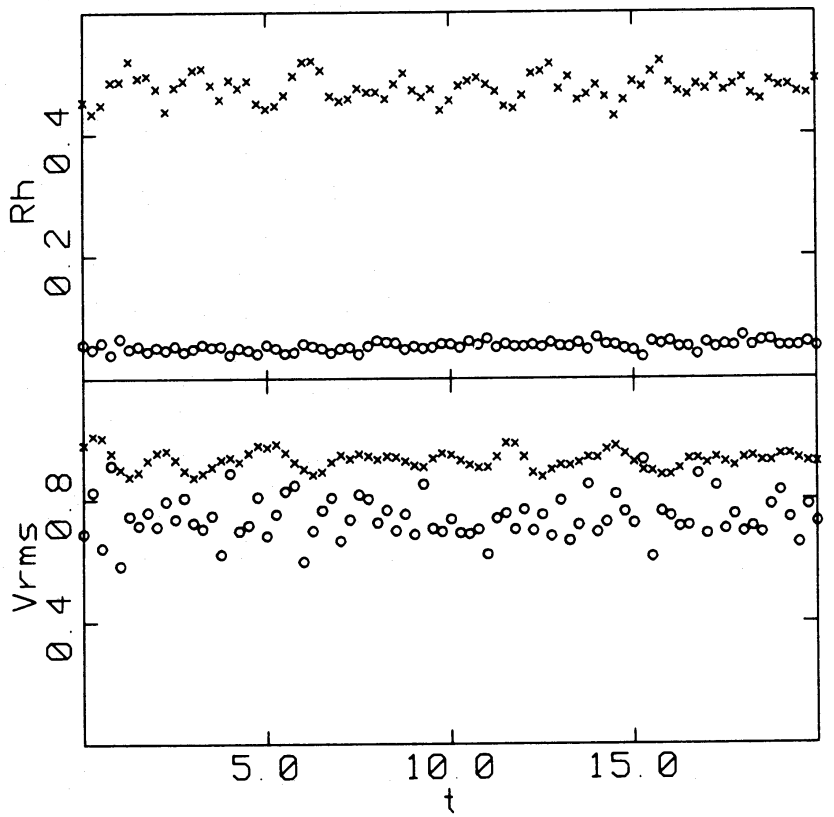

Figure 1. A stability test of galaxy model g_1. The upper panel shows the evolution of the half-mass radii of the core (circles) and halo (crosses), while the lower one shows the rms velocity dispersions. (In the units used in this figure, the model has mass $m_g=1$ and binding energy $e_g=-1/4$). Significant relaxation between the two components would cause the core half-mass radius to increase with time. The lower velocity dispersion of the core is a softening effect.

halo half-mass radius. Isolated galaxies constructed by this procedure were run for 20 halo crossing times; as Fig. 1 shows, there was no significant evolution over this time.

The initial conditions for a 'handmade' group of similar galaxies (differing only in the choice of generating random numbers) were partially specified by the following parameters and options:

(i) The initial number of galaxies, N_g.

(ii)The fraction F_b of the total mass placed in a common dark group background.

(iii) The internal binding energy of the galaxies, compared to the overall binding energy of the group. This was quantified by the parameter

$$\eta=\frac{(e_g/m_g)}{(E^*/M)}, \tag{2}$$

where e_g and m_g are the binding energy and mass of an isolated galaxy, and $E^*=T^*+U^*$ and M are the binding energy (computed after first replacing each galaxy with a point particle of equal mass) and mass of the entire group.

(iv) The overall dynamical state of the group; three options were considered. In 'virialized' groups the galaxies (and common background particles) were given isotropic velocity dispersions sufficient to make $T^*/U^*=-\frac{1}{2}$. Groups at 'turnaround' were similar, except that $T^*/U^*=-\frac{1}{8}$. Finally, in 'expanding' groups, random velocities were set to zero, and a uniform Hubble flow such that $T^*/U^*=-\frac{1}{4}$ was imposed.

Given these parameters, pseudo-random positions and velocities for the galaxy centres and common background particles were chosen from a 3-dimensional Gaussian, and scaled to satisfy (iv), while the internal scale of the galaxies was adjusted to comply with (iii). The entire system was then scaled to virial units, in which $E^*=-\frac{1}{2}$, $M=1$, and $G=1$; these units are natural ones for an observer who treats galaxies as particles.

The initial conditions generated in this manner (see Figs 2 and 3) are admittedly somewhat artificial; in real groups the galaxies span a wide range of masses, and the initial distribution of dark matter was probably much more irregular. The idealizations adopted in these models, however, simplify the task of understanding the physical mechanisms responsible for their evolution. These mechanisms approximate a subset of the physical mechanisms operating in real groups. Furthermore, in so far as real groups probably came from a wide range of initial conditions, the models presented here should be passable approximations of at least some groups.

An ensemble of several similar models, differing only in the generating sequence of random numbers, was run for each choice of parameters. Considerable variable was found from run to run within a given ensemble; by running ensembles instead of single models, the significance of apparent trends from one set of parameters to another could be evaluated. Table 2 lists parameters for the ensembles run. In all cases, the total luminous fraction was $F_l=f_l(1-F_b)=0.1$. The half-light radii of the cores was $r_{hl}\simeq 0.4F_l/\eta N_g=0.008$ in virial units, except for ensembles B and F, for which $r_{hl}\simeq 0.004$.

2.2 'NATURAL' INITIAL CONDITIONS

To explore the consequences of relaxing some of the idealizations attending the handmade models, a series of 'natural' models were also run. These natural runs attempted to simulate a White & Rees (1978) scenario, in which dark matters clusters hierarchically, creating dark haloes within which a gaseous, dissipational fraction $F_l\approx 0.1$ could cool, collapse and fragment, forming stars and galaxies. The simulations started with a homogeneous sphere of N particles, with Poisson fluctuations and uniform Hubble expansion, scaled to have binding energy $E=-1$, total

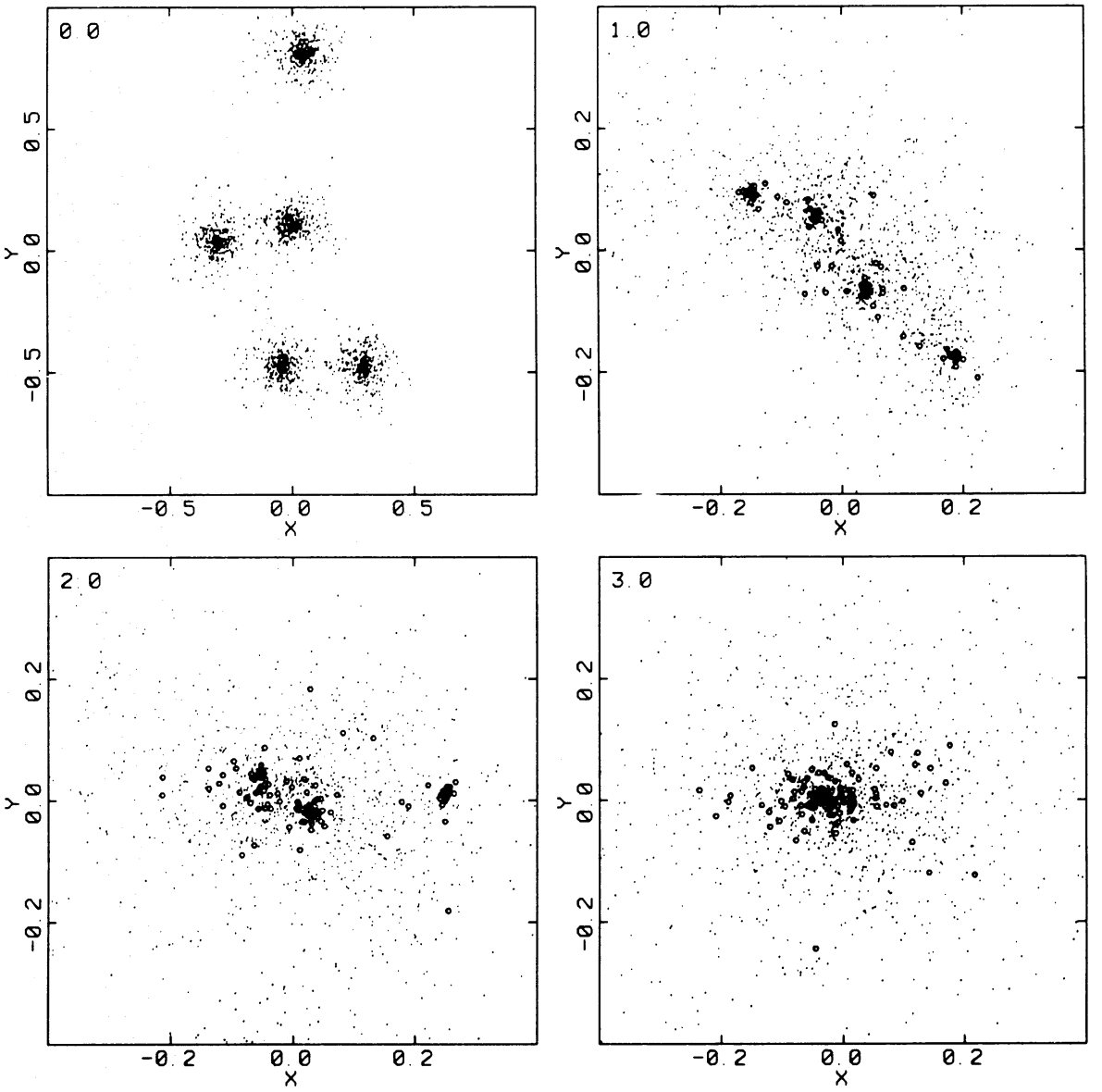

Figure 2. Snapshots from a run in ensemble C (F_b=0, turnaround). Times are as indicated; the scale changes between the first and second frames. Luminous particles are plotted as small circles, dark particles as points. The group collapses and forms a common halo by $t\approx1.0$; merging is essentially completed $t\approx3.0$.

mass $M=1$, and initial radius R_i. If this sphere remained completely homogeneous, it would have reached a maximum radius

$$R_m=\frac{3M^2}{5|E|}=0.6, \tag{3}$$

the time taken to do so from $R=0$ being

$$t_m=\pi\sqrt{\frac{27\ M^5}{1000\ |E|^3}}\simeq0.516 \tag{4}$$

At some chosen epoch t_{gf} when significant clustering had developed, a cluster-finding algorithm was used to identify clumps of particles. The 'critical-distance' algorithm used grouped particles into equivalence classes, where two particles were placed in the same class if (i) they were

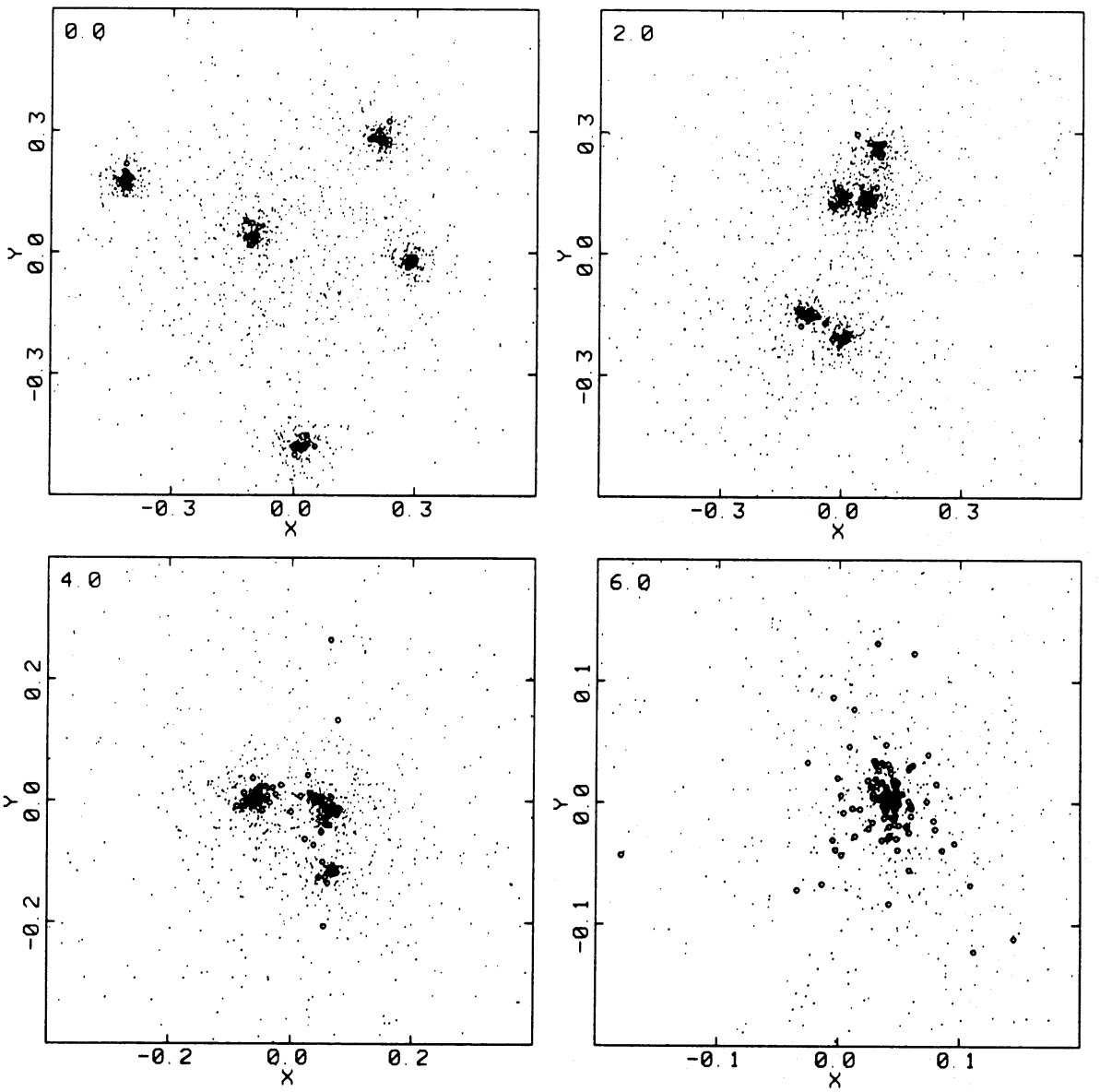

Figure 3. Snapshots from a run in ensemble E (F_b=0.5, virialized). The scale changes between the second, third and fourth frames. From the start until t≈3.5 the galaxies spiral toward the centre; by t≈5.0 only a binary is left, which decays by t≈6.0.

separated by less than d_c or (ii) one particle was a member of a class and the other was within d_c of any particle of that class. Clumps of $n_c \geq n_{min}$ particles became galaxies; in each clump the particles were sorted by potential energy, and the $(0.1N/N_c)n_c$ most bound particles were designated as luminous (where $N_c=\Sigma n_c$ is the total mass in galaxies). To simulate dissipation, the velocities of the luminous particles were set to zero with respect to their galaxy as a whole; these particles then collapsed and revirialized within their dark haloes.

Of course, this procedure is not completely satisfactory. Although the parameters d_c and n_{min} could usually be set so as not to link unrelated objects, some haloes had more than one potential centre. The dissipation scheme treated multiple centres incorrectly, attempting to merge them instead of allowing each to collapse independently. Furthermore, is not clear that enough 'dissipation' actually took place. Dissipation should properly be treated as an ongoing process; this can be approximated only by including non-gravitational terms in the equations of motion

Table 2. Parameters for handmade groups models. The turnaround time t_m is given in virial units (Section 2.1).

Ensemble	Runs	Galaxy	N_g	F_b	η	State	t_m
A	2	g_1	5	0	1	Vir.	0.516
B	2	g_1	5	0	2	Vir.	0.281
C	4	g_1	5	0	1	Turn.	0.516
D	1	g_1	5	0	1	Exp.	0.516
E	2	g_2	5	0.5	1	Vir.	0.794
F	2	g_2	5	0.5	2	Vir.	0.516
G	2	g_3	10	0.5	0.5	Vir.	1.04
H	4	g_2	5	0.5	1	Turn.	0.794
I	1	g_2	5	0.5	1	Exp.	0.794
J	3	g_4	5	0.75	1	Vir.	1.04
K	3	g_4	5	0.75	1	Turn.	1.04
L	1	g_4	5	0.75	1	Exp.	1.04

(Negroponte & White 1983). Finally, it is difficult to assess the effects of two-body relaxation; many of the galaxies had less than 50 particles altogether, and probably relaxed quite quickly. Despite these shortcomings, some galaxies settled down to more or less plausible core–halo systems which could be followed for a reasonable time.

2.3 OBSERVING THE SIMULATIONS

To extract quantitative results from the models, a procedure for 'observing' luminous particles and grouping them into cores was devised. The scheme used here was to apply the critical-distance algorithm (Section 2.2) to the luminous particles, with d_c chosen such that a specified fraction F_c of particles were linked to others. To reduce the numerical noise, three-dimensional coordinates were used; in addition, a number cut-off n_{cut} was used to reject isolated clumps of a few particles. This technique automatically recognized mergers between cores; it proved fairly reliable and insensitive to the parameters F_c and n_{cut} for cores containing 20 or more luminous particles. The parameter values F_c=0.75 and n_{cut}=10 gave stable results for the handmade models, generally agreeing with visual estimates. The natural models usually had a larger number of cores, with relatively few luminous particles in each, so n_{cut}=5 was chosen to make the most of the available particles. Any reasonable cluster-finding algorithm would probably yield similar results, although this scheme, which automatically ignores overall changes in scale, may yield more satisfactory results than, for example, an algorithm which identifies regions above some fixed critical density.

3 Results

3.1 HANDMADE MODELS

Figs 2 and 3 show snapshot sequences from runs in ensembles C (F_b=0, turnaround) and E (F_b=0.5, virialized) respectively. In Fig. 2 the rapid collapse following turnaround triggers a burst of merging, although several dynamical times are required to complete the process. As might be expected, the group shown in Fig. 3 evolves more slowly, although there is a significant element of chance in the evolution of any single model. The weakly hyperbolic collisions which occur in these models are ineffective at stripping the matter from haloes; instead, the haloes stick together on

encounter, and trap the cores, which quickly merge. Note that the merger remnant retains a core–halo structure as it grows, and that it quickly settles to the centre of the system. The remnant is very effective at catching other galaxies; very few groups formed more than one remnant.

Although snapshots provide a detailed description of the system at a given instant, they are of less help in understanding the sequence of events during a simulation. The observation procedure (Section 2.3) can be used to extract the number, positions, velocities and masses of the cores at frequent intervals. Fig. 4 shows radial coordinates of cores versus time for several models, including (Fig. 4a and 4d) the models presented in Figs 2 and 3. The area of plotting symbols used indicates the mass; cores in which the ratio of captured to original mass (see Roos & Aarseth 1982) is greater than 0.8 are plotted as circles. The two models starting from turnaround, 4a (F_b=0) and 4c (F_b=0.5) yield similar results. After the initial collapse, the cores are trapped in the centre, having expended kinetic energy in disrupting their haloes and /or stirring up the common

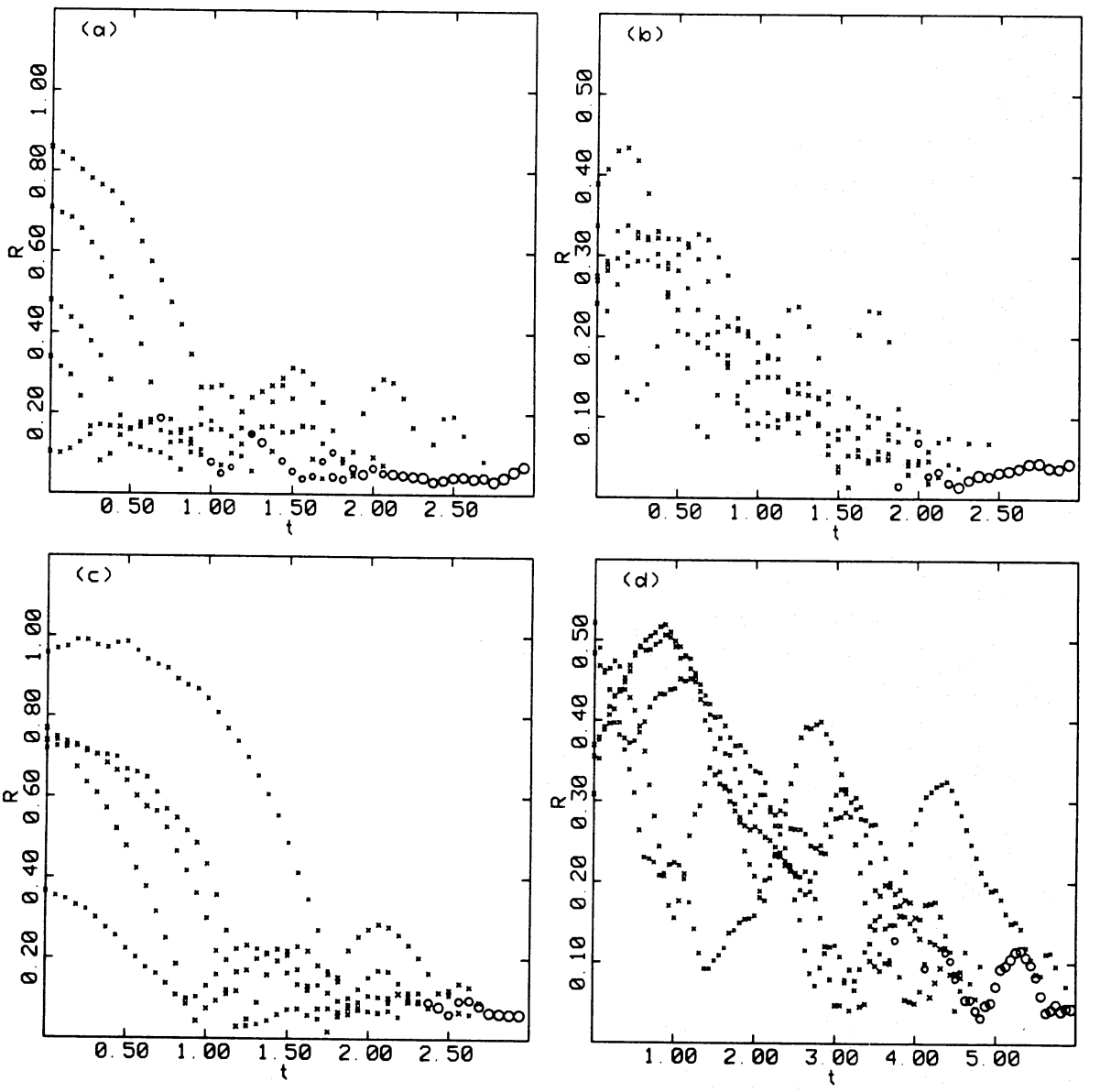

Figure 4. Radial trajectories of cores from runs in ensembles C (4a). A (4b), H (4c), and E (4d). The models shown in 4a and 4d are the same as those in Figs 2 and 3. The area of plotting symbols is proportional to mass; cores with substantial merged mass are plotted as circles.

halo; their orbits then decay until they merge. In the initially virialized model of 4b all the dark mass was placed in galaxy haloes; as a result, the galaxies interact violently, making it difficult to trace individual trajectories. The overall contraction of the system is a result of these interactions, which transfer energy from the orbital motions of galaxies to internal motions within galaxies (Biermann & Wielen 1978; Carnevali *et al.* 1981). The initially virialized model of 4d, with less dark mass in galaxies, yields smoother orbits and takes twice as long to merge completely (this was one of the longest lived runs). Both dynamical friction and galaxy–galaxy interactions appear to contribute to the decay of the orbits; in particular, the last surviving galaxy spirals in very much as expected from dynamical friction.

Fig. 5 presents merging histories for the ensembles listed in Table 1. Although the history varies considerably among runs within a given ensemble, on comparing different ensembles some interesting trends appear. First, turnaround and expanding models (5a, 5c, and 5e) generally merge rapidly as soon as the group collapses, whereas virialized models merge more gradually.

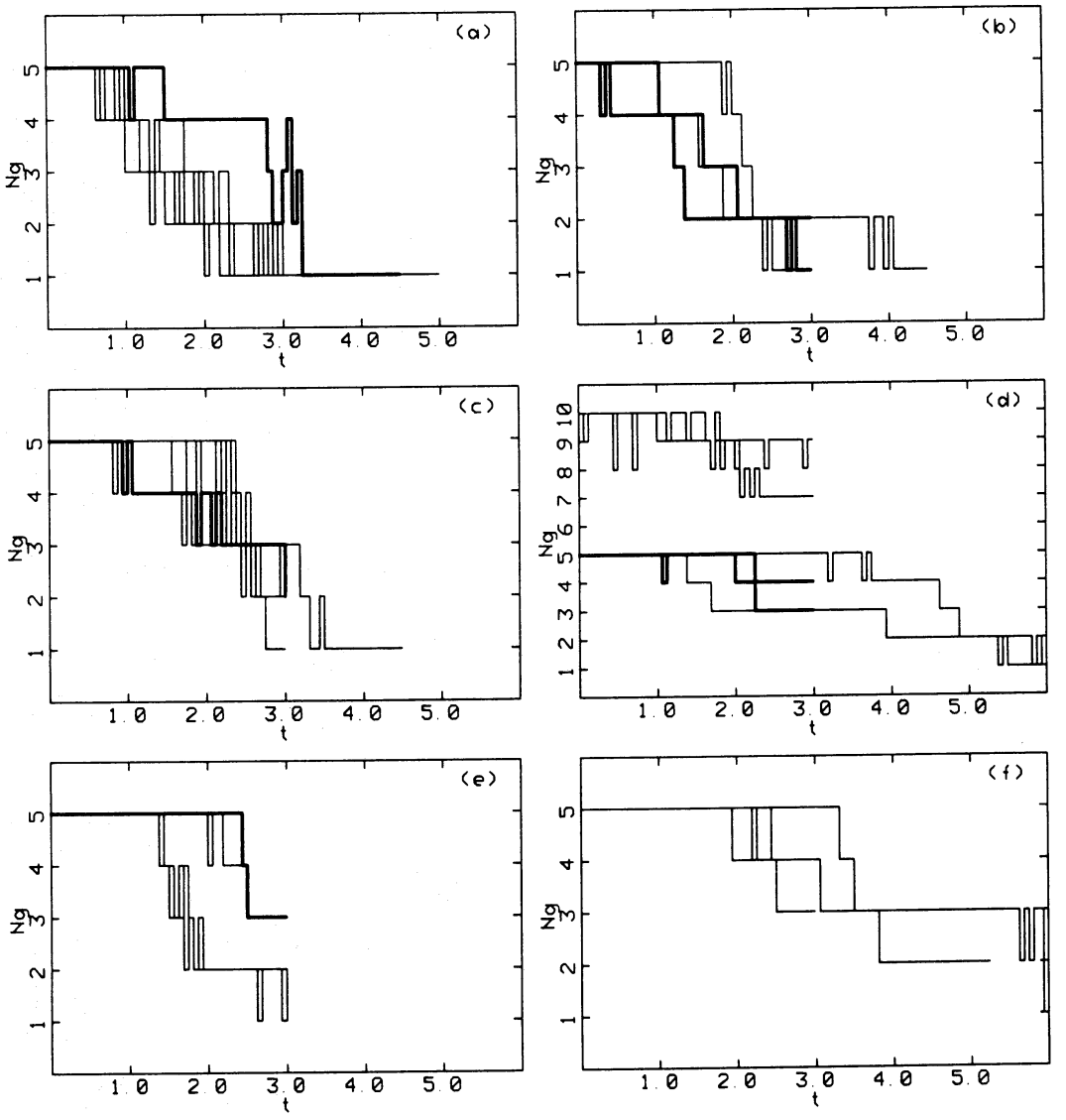

Figure 5. Merging histories, shown by number of cores versus time. The left-hand column shows turnaround and expanding (heavy line) models; the right-hand column shows virialized models including those with $\eta=2$ (heavy lines). The fractional mass in the common background, F_b, increases from 0 to 0.5 to 0.75 moving down the page. The scale in 5d is compressed to allow for ensemble G.

Secondly, ensembles B and F, with tightly bound galaxies (heavy lines in 5b and 5d), merge just as rapidly as ensembles A and E; this is unexpected, since making the galaxies more tightly bound reduces their geomerical cross-section. However, tightly bound galaxies have higher internal velocity dispersions, and therefore respond *more* violently to low-velocity encounters; the increased response per collision may compensate for small cross-sections. Thirdly, the merging rate is generally reduced if more mass is initially placed in a common group halo; this result may be understood by noting that the mass in the common halo was taken from individual galaxy haloes, reducing their cross-sections without changing their velocity dispersions. In ensembles F and G, approximately 20 per cent of the galaxies escaped from the inner group on bound but long-period orbits; these may be examples of ejection by 2-body interactions, although the escapees were generally among the less tightly bound galaxies initially. However, even excluding these galaxies, the models with a common halo exhibit less merging. In principle, it might be possible to

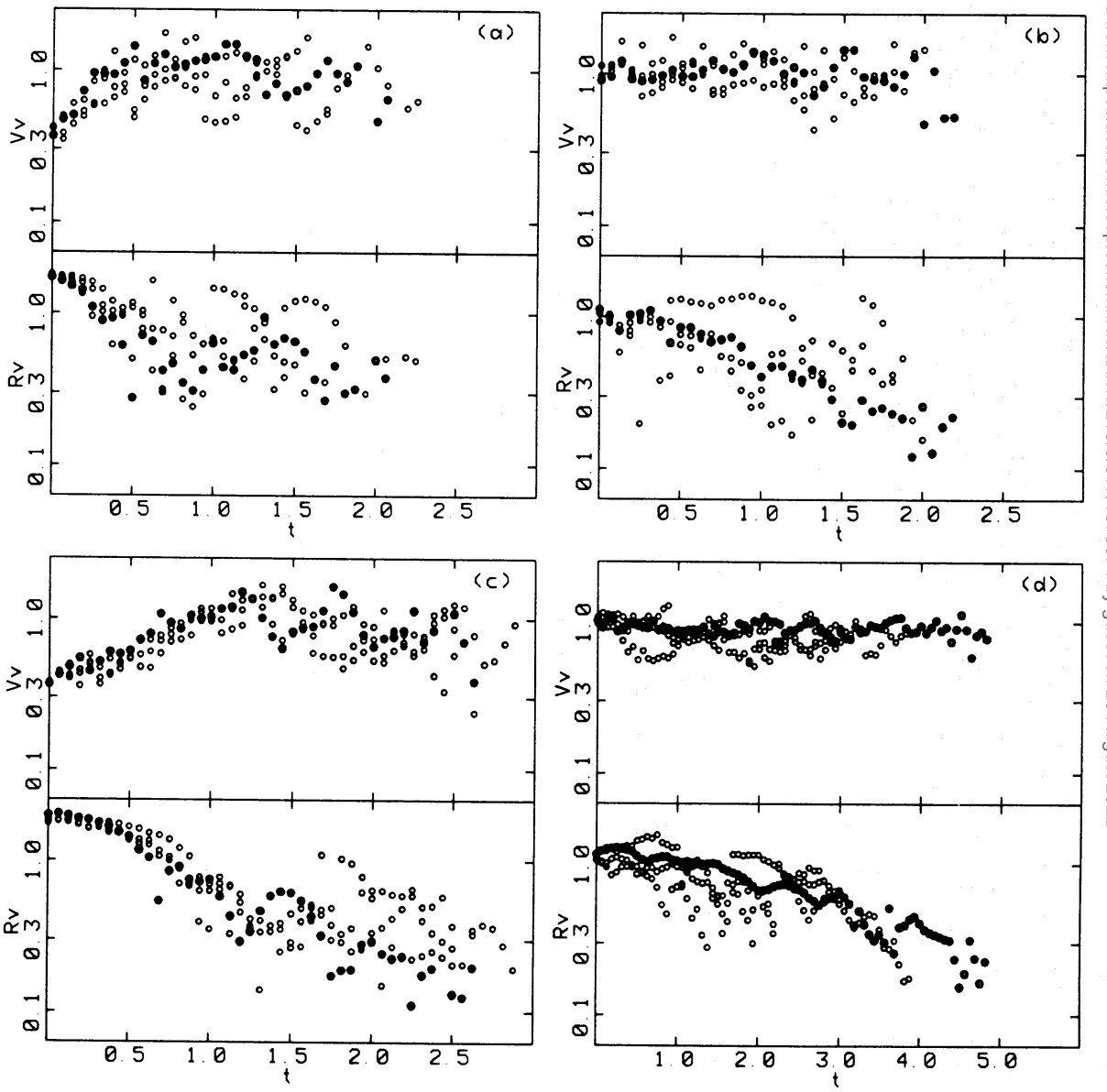

Figure 6. Apparent virial radii R_v and velocities V_v, derived from the observed cores and plotted versus time, for all runs in ensembles C (6a), A (6b), H (6c), and E (6d). Filled circles indicate results for the individual runs of Fig. 4. Ensembles with $\eta=2$ or $F_b=0.75$ yield results similar to those shown for ensembles with $\eta=1$ or $F_b=0.5$ respectively.

further delay merging by reducing the total luminous fraction, or by increasing the relative binding energy of the cores. These measures can only extend the interval between the initial halo encounters and the final merger; since the sticky haloes create a bound subsystem with a relatively short dynamical time, the overall effect is probably small.

Determination of the virial parameters provides the basis for most dynamical studies of groups of galaxies. Corresponding model parameters were obtained from the instantaneous core positions $\mathbf{r}_i$, velocities $\mathbf{v}_i$ and masses m_i, using the estimators for R_V and V_v discussed in the Appendix. Figs 6 and 7 show the time evolution of the virial parameters for representative turning and virialized ensembles. The scaling adopted in Section 2.1 implies that the equilibrium values of R_v and V_v are unity, as are the virial mass $M_v \equiv V_v^2 R_v$ and virial crossing time $T_v = R_v/V_v$.

The results presented in Figs 6 and 7 show that dynamical evolution strongly influences the apparent virial parameters of groups of galaxies. Models starting at turnaround initially yield results typical of any collapsing system: the virial radius and velocity start on opposite sides of equilibrium but exchange places before maximum collapse. In contrast to what is seen in a system

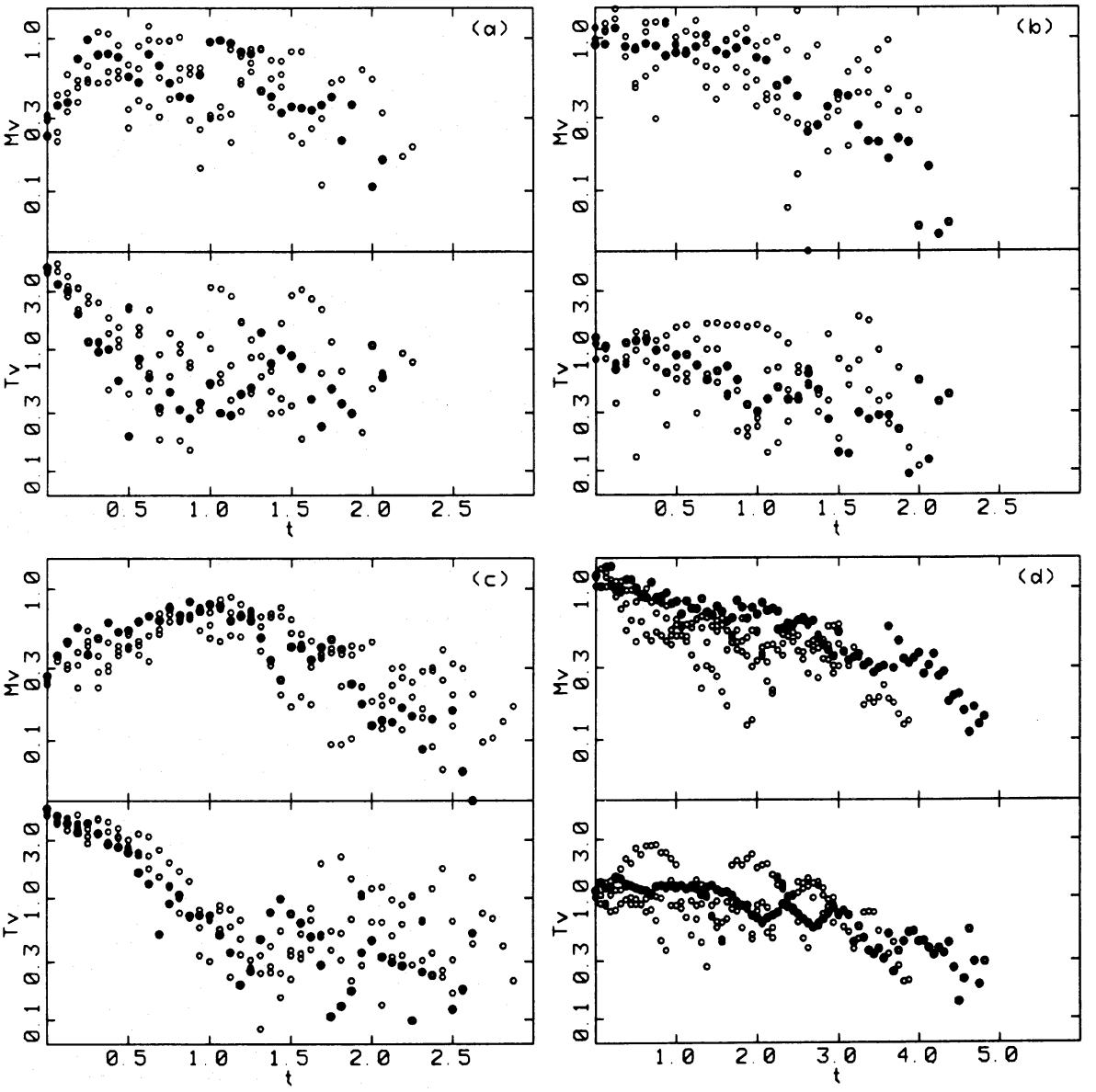

Figure 7. As for Fig. 6, but showing apparent virial times T_v and masses M_v.

of point masses, the virial radius does not bounce back to equilibrium following collapse. Models started from approximate equilibrium generally evolve more slowly, the virial radius of the group systematically decreasing as the cores spiral in to the centre. It is interesting that the virial velocities show very little evolution; a similar result has also been found in more idealized N-body models (Barnes 1984b). In later evolutionary stages, the virialized, turnaround and expanding models all yield virial mass estimates consistently lower than the total mass of the group. This primarily reflects the segregation, induced by gravitational interactions, between the galaxies and the dark matter, and should also apply to other dynamical mass estimates, including the projected mass method of Bahcall & Tremaine (1978). In advanced stages of evolution the cores appear to form an 'inner group' for which virial analysis yields noisy but relatively unbiased results. The virial mass may be compared to the total mass of the system *within* some radius characteristic of the cores; typically M_v is at least twice the total mass within the group half-light radius, but less than the total mass within the outermost galaxy (*cf.* Hoffman, Shaham & Shaviv 1982). The conclusion is that virial analysis yields reasonable results for the visible part of a group, but consistently underestimates the total mass of the system which gave rise to that group.

To some degree, the turnaround and virialized models simply explore different phases of group evolution. Like the turnaround models, real groups probably underwent significant radial collapse following maximum expansion; the models show that galaxy haloes would have been partially disrupted during this collapse. The visible cores, still retaining some of their original halo matter, would then have been trapped at the bottom of the group potential well, within a common envelope of dark matter. At this point, such groups roughly resemble the initial conditions taken from the virialized models with a common dark background; while the preceding collapse would have left a common halo of dark matter extending well beyond the galaxies, this extra mass is unlikely to have much further effect on the dynamics of the inner group. Collapsed groups probably evolve through the same mechanisms, dynamical friction and interactions between galaxies, responsible for the evolution of the virialized models with $F_b>0$. As long as a group retains some substructure (e.g. distinct galaxies), the time-scale for further dynamical evolution will be of the same order as the virial crossing time T_v; since dynamical evolution decreases T_v, a 'runaway' ensues, ending when the galaxies have merged (Carnevali *et al.* 1981).

3.2 NATURAL MODELS

The natural models were much less controlled than the handmade models, and considerable experimentation with different parameter values was required before 'successful' results were obtained. It proved difficult to obtain the large, well-defined clumps needed to mock up dissipation unless galaxy formation was delayed until approximately the turnaround time t_m. The choice of softening parameters was also critical, demanding a compromise between resolution, two-body relaxation, and computing time. Nevertheless, these simulations are of some help in relating the idealized models to the real Universe; so a single successful run will be presented in some detail to illustrate what can happen.

The model described here had $N=2000$ particles and was started at an initial radius $R_i=0.1$. At $t_{gf}=0.625$, slightly after maximum expansion in the homogeneous case, twelve clumps selected using $d_c=0.02$ and $n_{min}=20$ (comprising roughly a third of the total mass) were identified as galaxies, and a total of 200 particles apportioned according to halo mass were designated as luminous. The luminous particles, with peculiar velocities set to zero, quickly collapsed in their haloes, but did not build up sufficient velocity dispersion when compared to the system as a whole. Therefore, at $t=0.6875$, the peculiar velocities of the luminous particles were again set to zero; by $t=0.75$ the cores had again collapsed and finally reached acceptable velocity dispersions, scattered around unity. The smaller cores then had half-light radii of $r_{hl}\approx 0.002$, still somewhat

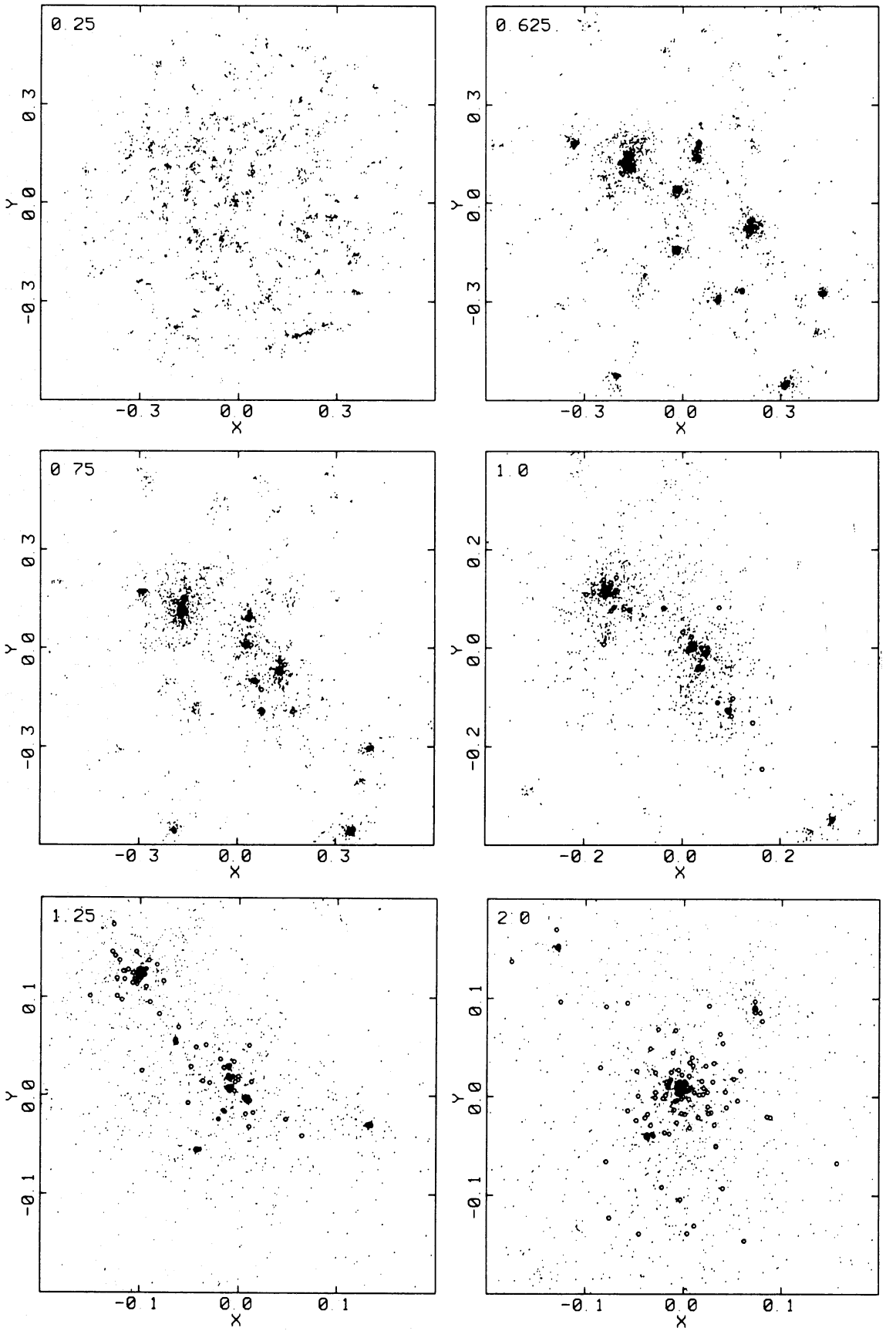

Figure 8, Snapshots from the natural model. The scale changes between the third, fourth and fifth frames. Luminous particles are selected at t_{gf}=0.625 and subsequently plotted as circles; each clump of luminous particles is a core. By $t \approx 1.0$ the group of small galaxies at the lower right has collapsed and created a common dark halo; merging is underway in the next frame, while the last frame shows the final remnant with several satellites.

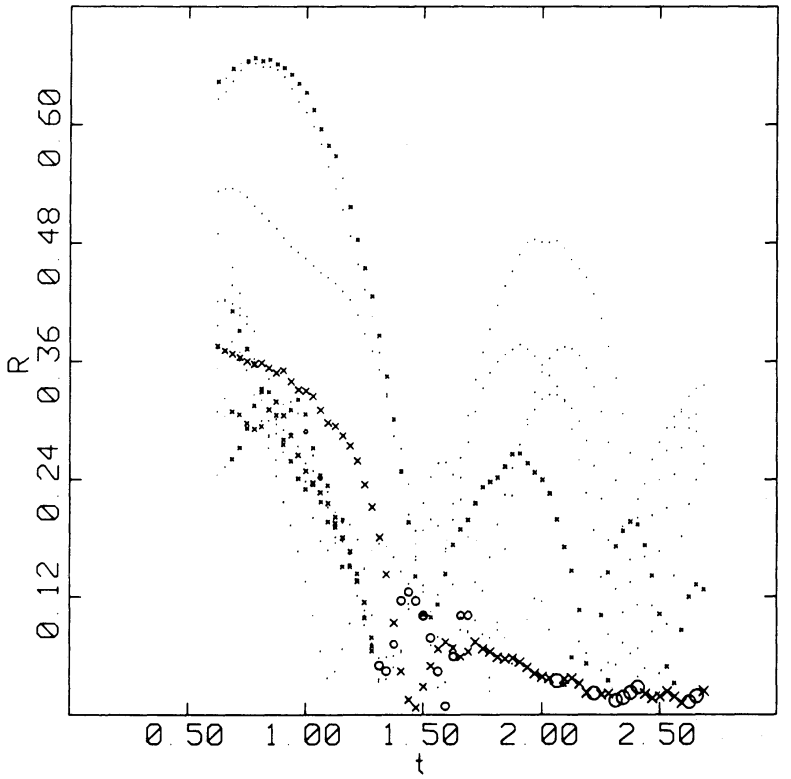

Figure 9. Radial trajectories of cores in the natural model. The symbols are as in Fig. 4, with low-mass galaxies plotted as points. The first significant merger remnant forms at $t\approx1.3$ and mergers with a comparable galaxy (the largest in the initial conditions) at around $t\approx1.7$.

greater than the luminous softening parameter, $\varepsilon_l=0.001$ (the dark particles having $\varepsilon_d=0.01$). With such small softening, the N-body integration proceeded rather slowly.

Fig 8 presents a series of snapshots of this run. The first frame shows the system well before galaxy formation, while the next frame shows the instant of formation, the luminous particles not yet having collapsed in their haloes. In the third frame the cores have settled to their final radii, and at the same time a subgroup of six galaxies, slightly to the right and below the centre, has begun to collapse. By the next frame this subgroup has more or less settled down in a common halo and the cores have started to merge; merging is completed shortly after the fifth frame, the remnant falling toward the largest galaxy (upper left). These two objects merge around $t\approx1.7$ (not shown); the last frame shows the final remnant, surrounded by five satellite galaxies.

This sequence of events is largely recapitulated in Fig. 9, which plots the radial coordinates of the cores versus time. Dots denote cores of less than ten particles, while other symbols are as in Fig. 4. Around $t\approx1.5$, the merged subgroup (plotted as a circle) and the largest galaxy have formed an approximately equal-mass binary, which manages a couple of orbits before itself merging. This plot also shows the plunging orbits of the satellite galaxies, which appear to decay, probably through dynamical friction.

A virial analysis of this run is complicated by the changing morphology; the initial system is essentially a group, which then turns into a binary, and finally becomes either a cD in a poor group, or perhaps a bright elliptical with satellites. Fig. 10 shows virial parameters versus time, using the same techniques as in the last section. These results are probably most relevant to groups of galaxies before $t\approx1.5$, while after $t\approx1.7$ a projected-mass analysis (Bahcall & Tremaine 1978) might be more appropriate. On the whole Fig. 10 recalls the virial evolution of the handmade ensembles started at turnaround; the same pattern appears, with both the virial mass and time-scale being significantly underestimated.

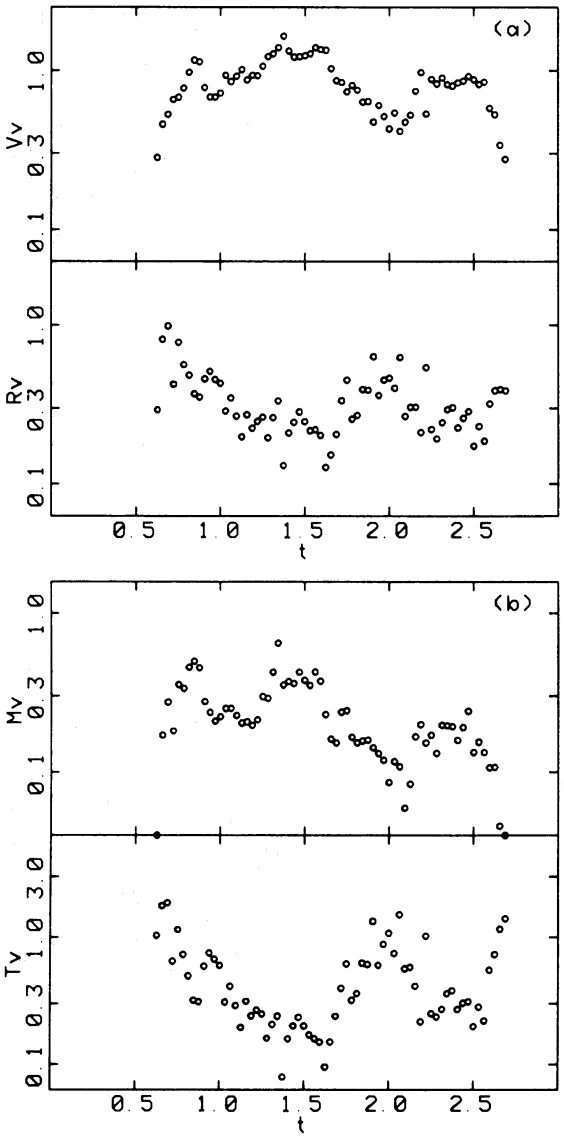

Figure 10. Virial parameters from the natural model, computed as for Figs 6 and 7. Virial analysis can only be strictly applied before $t \approx 1.5$ because of the changing morphology of the system. In general the pattern up to this time recalls the virial results from the ensembles started at turnaround.

4 Comparison with observations

Are the models presented here consistent with real groups of galaxies? Groups have such diverse properties that the question is almost meaningless; one must first narrow down the scope of the comparison. For simplicity, consider only the models starting from turnaround, and ask if such models can be consistent with groups for which the (H_0-independent) parameter $T_v H_0 \approx 0.1$. This is an interesting test for two reasons. First, while turnaround models have the more plausible initial conditions, they also merge quickly, and thus could well fail to 'live' long enough. Secondly, groups with $T_v H_0 \approx 0.1$ should be well past the collapse stage and thus are often considered good candidates for virial analysis (Gott & Turner 1977).

To determine when a model is consistent with $T_v H_0 \approx 0.1$, one can in principle simply compare the value of T_v estimated from the cores with the model's cosmological age t_0. Here $t_0 \equiv t + t_{start}$, where t is the elapsed simulation time and t_{start} is the time that would have been required, starting from the Big Bang, for the model to reach the point of turnaround. Approximate limits on t_{start}

may be derived by assuming that at early epochs the model group was a nearly spherical perturbation with fixed mass M and binding energy E. Had it remained homogeneous sphere, the time to turnaround would be t_m as given by equation (4); in the units used here, $E=0.5[1+(1-F_b)\eta]$, and t_m is listed in Table 2. The growth of substructure (such as galaxies) will lock up some of the total binding energy E and thus delay turnaround; a plausible upper bound, $t_m^*\simeq 1.46$, is obtained by replacing E in equation (4) with $E^*=0.5$, the binding energy *neglecting* substructure. (Fig. 9 shows an example of a closely related effect: for this model $t_m\simeq 0.516$, yet maximum collapse comes around $t\approx 1.5$ instead of the naïvely expected time $2t_m$.) Thus,

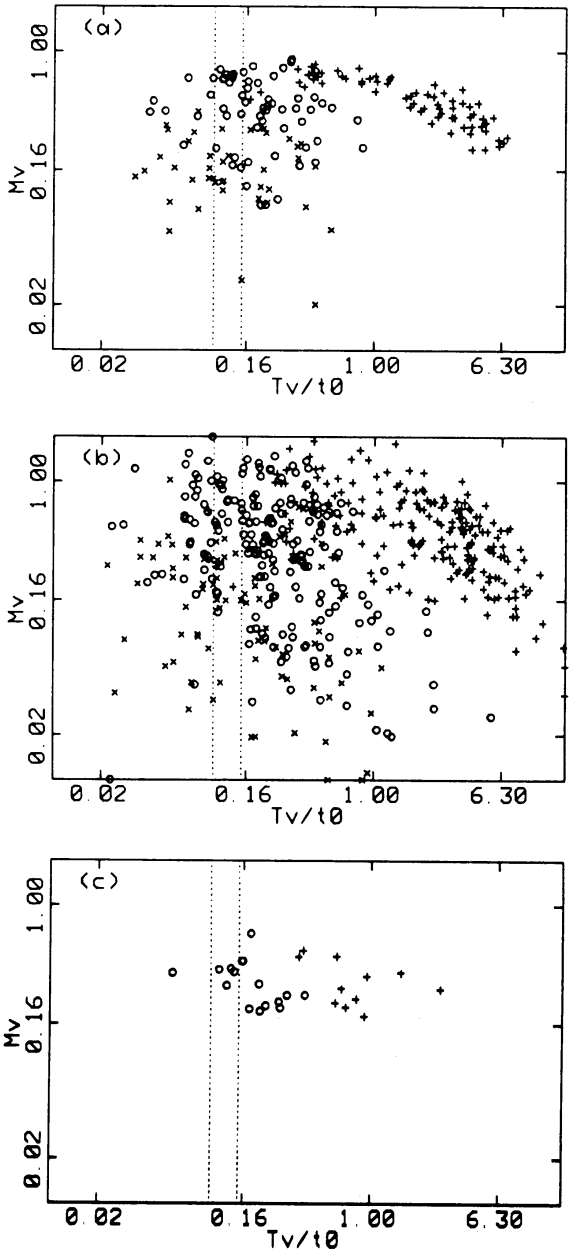

Figure 11. Model results plotted on M_v versus T_v/T_0 plane. 11a gives results for ensemble H, computed assuming $t_{start}=t_m$; plotting symbols +, ○ and × denote the time ranges $0.8\leqslant t_0<1.8$, $1.8\leqslant 2.8$ and $2.8\leqslant t_0<3.8$ respectively. 11b shows the corresponding results derived from three orthogonal projections of the same ensemble. 11c gives results for the natural model; symbols + and ○ denote $0.625\leqslant t_0<1.0$ and $1.0\leqslant t_0<1.5$. The dotted lines delimit the region corresponding to $T_vH_0\approx 0.1$ for $0\leqslant\Omega\leqslant 1$.

$t_m \lesssim t_{start} \lesssim t_m^*$. A further complication involves the conversion from cosmological time t_0 to H_0; this is $H_0 = 1/t_0$ if $\Omega \ll 1$ but $H_0 = 2/3t_0$ if $\Omega = 1$.

Fig. 11 gives results from several ensembles plotted on the T_v/t_0 versus M_v plane. Models started at turnaround with $F_b = 0.5$ are shown in Fig. 11a, computed using the lower (more critical) limit, $t_{start} = t_m$. Such models first become consistent with $T_v H_0 \approx 0.1$ not long after the initial collapse, for either choice of t_{start}, as do models with $F_b = 0.75$. On the other hand, the models starting from turnaround with $F_b = 0$ (not plotted) merge before getting old enough, unless $t_{start} = t_m^*$ and $\Omega = 1$. To show the effect of projection, Fig. 11b shows the corresponding results obtained from three orthogonal directions, with R_v and V_v corrected by the usual factors of $\pi/2$ and $\sqrt{3}$. While the scatter is increased, the overall pattern is much like 11a. Finally, 11c shows results for the natural model with t_{start} accurately taken equal to zero; this model appears consistent at the later stages of group evolution, although little weight can be placed on one experiment.

Models which have evolved to $T_v H_0 \approx 0.1$ typically have virial radii $R_v \approx 0.4$, while the half-light radii of the cores are $r_h \approx 0.008$. Typical bright galaxies have half-light radii $r_h \approx 3$ kpc; the model galaxies are thus somewhat more extended than real ones unless the group models are scaled to have virial radii of 0.1–0.2 Mpc, which are somewhat small but not uncommon. More compact galaxies would be less susceptible to merging, but this effect should not be very strong since, as noted above, the merging rate is controlled by the short dynamical time-scales of the compact subgroups formed when haloes stick together. To reduce the core half-light radii without inflating the core velocity dispersions, the overall fraction of luminous mass would have to be taken of order 0.02–0.05 instead of the cannonical 0.1; while such lower values may even be preferable in a high-Ω universe, they would be much more difficult to simulate with equal-mass particles.

On the whole, there is no difficulty in finding models starting from turnaround consistent with $T_v H_0 \approx 0.1$, even among those which have collapsed relative recently. This is, in part, because such models already show significant dynamical evolution, lowering the apparent value of T_v. These models typically yield virial masses roughly a third the total value; in addition, most have had at least one merger.

5 Implications of group evolution

The models described here all evolve significantly within a few crossing times. In models starting from turnaround, considerable merging and disruption of dark haloes takes place during the initial collapse. In this process the cores expend kinetic energy and are therefore unable to get away from each other following collapse. Virialized models evolve more smoothly, especially if some of the dark mass is initially placed in a common halo. Galaxy–galaxy interactions and dynamical friction both conspire to extract energy from the orbital motion of the cores, which collect at the centre of the system. The dynamical evolution of these models can be viewed as a *dissipative* process: the initial coherent motions of galaxies are converted to random motions of stars and dark matter (in effect, into heat).

The application of these results to real groups is somewhat complicated by uncertainties in the observational data and in the appropriate initial conditions. However, from the discussion of Section 4, it appears that groups with crossing times $\sim 0.1 H_0^{-1}$ are not the stable, relaxed systems that one might naïvely expect. In one sense, such groups are younger than expected, in that they have probably only just collapsed, while in another sense they are older than expected, having already undergone considerable dynamical evolution. It seems unrealistic to describe groups as equilibrium systems; present-epoch groups must have looked quite different at $z = 1$, and will probably have changed out of recognition in another Hubble time. Most groups should already have had a few mergers. Evidence for merging in typical groups is controversial: McGlynn & Ostriker (1980) found a significant correlation between dynamical time-scales and the promi-

nence of the brightest galaxy, but Mardirossian, Giuricin & Mezzetti (1983), have argued that this correlation is spurious. Hickson (1982) noted that while compact groups have fewer spirals than the general field, the brightest galaxy is just as likely to be spiral as elliptical, and therefore is not a merger remnant.

Is it possible that evidence for merging in groups has been overlooked? First, most studies have assumed that the brightest galaxy is the cannibal, but in the natural run above, the first significant mergers occur in a subgroup of small galaxies, the largest galaxy present remaining aloof. Large galaxies would not always be the most successful cannibals if they tended to form in isolation, having depleted their surroundings. It is worth noting that Hickson (1982) found that the more compact of his groups contain fewer faint galaxies and more ellipticals. Secondly, many mergers probably involve galaxies of unequal masses; mergers between giant disc galaxies and dwarf galaxies (of any type) may yield early-type disc systems or S0 galaxies, instead of the elliptical star-clouds produced by equal-mass mergers. Only at very high densities are giant galaxies likely to encounter each other; this is in qualitative agreement with Dressler's (1980) density–morphology relationship. Thirdly, while spirals have not (yet) been produced by merging in N-body experiments, a merger remnant could acquire a disc, and thus disguise itself as an early S or S0. There are indications (see Gunn 1981) that galactic discs are accreting gas today, and there is no obvious reason why the same could not happen to an elliptical [although Barnes & White (1984) argue that this process alone cannot account for typical disc galaxies].

Unless rather special cosmological initial conditions are assumed, groups of galaxies have probably been forming for a considerable fraction of a Hubble time, and groups in advanced evolutionary stages should be common. Although spectacular examples such as V Zw 311 (Schneider & Gunn 1982) can be found, they appear to be relatively rare. Estimates of the relative number densities of compact groups and possible group remnants could set interesting constraints on the kind of models presented here. One uncertainty concerns the nature of the remnant; should one look for bizarre objects, cD galaxies in poor clusters, or ordinary bright ellipticals?

Rich clusters, because of their higher velocity dispersions, are not presently subject to the mechanisms which drive evolution in small groups. In a hierarchical scenario, however, rich clusters would have formed by the amalgamation of smaller ones (Layzer 1954; White 1976); these smaller clusters could well have undergone significant evolution before merging. Merritt (1985) has argued that cD galaxies are unlikely to have formed directly in rich clusters, but could have formed in groups or poor clusters, conceivably via the evolutionary processes described here. Rich clusters may also have inherited some segregation between galaxies and dark matter from their progenitors, since merging does not completely wipe out radial gradients (White 1978, 1979). Group evolution could thus have indirectly influenced the properties of rich clusters.

Group evolution promotes segregation between galaxies and dark matter, so dynamical mass estimators, when applied to evolved groups, generally yield underestimates. This effect may explain why groups have smaller M_v/L ratios than rich clusters (Hoffman *et al.* 1982; Barnes 1983). If segregation can 'bootstrap' up to rich clusters, even these systems may imply the existence of more dark mass than is indicated by virial estimates. Estimates of Ω from the virial masses of groups and clusters should thus be regarded as lower limits. Acting in concert with mechanisms which could have 'built in' segregation at the epoch of galaxy formation (Kaiser 1984), group evolution may help to reconcile the observational data with the theoretical prejudice that $\Omega=1$.

The effect of group evolution on large-scale structure has yet to the studied, although Aarseth & Fall (1980) and Roos (1981) have included merging rules in cosmological N-body experiments. Segregation and merging will have opposite effects on the two-point correlation function $\xi(r)$ at small scales, and it is not clear which effect would dominate; the scope of such effects could be

roughly delineated from the fractional contribution to ξ from pairs of galaxies within the same group. With the codes and computers now becoming available, it may soon be possible to address the problem of group evolution and large-scale structure by the techniques used in this study. In particular, experiments along the lines of the natural models, with more realistic techniques for including dissipation, could shed considerable light on the distribution of dark matter.

Acknowledgments

I thank numerous colleagues for invaluable discussions over the course of this project. Code development was supported in part by NSF grant AST-8114715; the Berkeley Astronomy Department provided $\sim 10^{13}$ floating point operations.

References

Aarseth, S. J. & Fall, S. M., 1980. *Astrophys. J.*, **236,** 43.
Arp, H., 1966. *Astrophys. J. Suppl.*, **14,** 1.
Bahcall, J. N. & Tremaine, S., 1978. *Astrophys. J.*, **244,** 805.
Barnes, J., 1983. *Mon. Not. R. astr. Soc.*, **203,** 223.
Barnes, J., 1984a. *PhD thesis*, University of California, Berkeley.
Barnes, J., 1984b. *Mon. Not. R. astr. Soc.*, **208,** 873.
Barnes, J. & White, S. D. M., 1984. *Mon. Not. R. astr. Soc.*, **211,** 753.
Biermann, P. & Wielen, R., 1978. In: *Large Scale Structure of the Universe*, eds Longair, M. S. & Einasto, J., Reidel, Dordrecht, Holland.
Carnevali, P., Cavalere, A. & Santangelo, P., 1981. *Astrophys. J.*, **249,** 449.
Dressler, A., 1980. *Astrophys. J.*, **236,** 351.
Gott, J. R. & Turner, E. L., 1977. *Astrophys. J.*, **213,** 309.
Gunn, J. E.. 1981. In: *Cosmology & Fundamental Physics*, (*Scr. varia. Pont. Acad. Sci.* **48**), 233.
Hickson, P., 1982. *Astrophys. J.*, **255,** 382.
Hoffman, Y., Shaham, J. & Shaviv, G., 1982. *Astrophys. J.*, **262,** 413.
Ishizawa, T., Matsumoto, R., Tajima, T., Kageyama, H. & Sakai, H., 1983. *Publs astr. Soc. Japan*, **35,** 61.
Kaiser, N., 1984. Paper presented at the *Inner Space–Outer Space* conference, Fermilab.
King, I. R., 1966. *Astr. J.*, **71,** 64.
Layzer, D., 1954, *Astr. J.*, **59,** 170.
Layzer, D., 1977. *CfA Preprint 850.*
Mardirossian, F., Giuricin, G. & Mezzetti, M., 1983. *Astr. Astrophys.*, **126,** 86.
McGlynn, T. A. & Ostriker, J. P., 1980. *Astrophys. J.*, **241,** 915.
Merritt, D., 1985. *Astrophys. J.*, **289,** 18.
Negroponte, J. & White, S. D. M., 1983. *Mon. Not. R. astr. Soc.*, **205,** 1009.
Roos, N., 1981. *Astr. Astrophys.*, **95,** 349.
Roos, N. & Aarseth, S. J., 1982. *Astr. Astrophys.*, **114,** 41.
Schneider, D. P. & Gunn, J. E., 1982. *Astrophys. J.*, **263,** 14.
Vorontsov-Vel'yaminov, B. A., 1959. *Atlas and Catalogue of Interacting Galaxies*, Vol. 1, Sternberg Institute, Moscow.
White, S. D. M., 1976. *Mon. Not. R. astr. Soc.*, **177,** 717.
White, S. D. M., 1978. *Mon. Not. R. astr. Soc.*, **184,** 185.
White, S. D. M., 1979. *Mon. Not. R. astr. Soc.*, **189,** 831.
White, S. D. M. & Rees, M. J., 1978. *Mon. Not. R. astr. Soc.*, **183,** 341.

Appendix: Choice of estimators for R_v and V_v

By definition, the instantaneous virial radius and virial velocity of an N-body system are

$$R_v \equiv -\frac{GM^2}{U} = \left(\sum_i^N m_i\right)^2 \Big/ \left(\sum_{j<i}^N \frac{m_i m_j}{r_{ij}}\right), \tag{A1}$$

$$V_v^2 \equiv \frac{2T}{M} = \left(\sum_i^N m_i(\mathbf{v}_i - \bar{\mathbf{V}})^2\right) \Big/ \left(\sum_i^N m_i\right), \tag{A2}$$

where $r_{ij} \equiv |\mathbf{r}_i - \mathbf{r}_j|$, and $\bar{\mathbf{V}}$ is the centre-of-mass velocity of the entire system. For equal-mass particles, (A1) reduces to $R_v = 2/\langle 1/r_{ij} \rangle$, neglecting a factor of $N/(N-1)$.

In practice, not all N particles may be observable. Suppose the $n \ll N$ particles which are observed are a 'fair sample' of the system. First, to estimate R_v, note that $\langle 1/r_{ij} \rangle_{obs} \approx \langle 1/r_{ij} \rangle$, so for equal-mass particles,

$$R_v \approx \frac{2}{\langle 1/r_{ij} \rangle_{obs}} = n(n-1) \Big/ \left(\sum_{j<i}^{n} \frac{1}{r_{ij}} \right). \tag{A3}$$

A reasonable generalization of (A3) to unequal masses is

$$R_v \approx 2 \left(\sum_{j<i}^{n} m_i m_j \right) \Big/ \left(\sum_{j<i}^{n} \frac{m_i m_j}{r_{ij}} \right). \tag{A4}$$

If there is no mass segregation among the particles, in the sense that $m_i m_j$ is uncorrelated with $1/r_{ij}$ (regression slope zero), then (A3) and (A4) are unbiased estimators of each other [although, when $n = N$, (A4) does not reduce to (A1)]. Secondly, to estimate V_v, equation (A2) may be used, *provided* that $\bar{\mathbf{V}}$ is independently known. If $\bar{\mathbf{V}}$ must be estimated from the observed particles, then $\langle (\bar{\mathbf{V}} - \bar{\mathbf{V}}_{true})^2 \rangle$ will typically be of order V_v^2/n, and (A2) will yield a systematic underestimate of V_v. If all particles have the same mass,

$$V_v^2 \approx \frac{1}{n-1} \sum_{i}^{n} (\mathbf{v}_i - \bar{\mathbf{V}})^2, \quad \text{where} \quad \bar{\mathbf{V}} \equiv \frac{1}{n} \sum_{i}^{n} V_i, \tag{A5}$$

is unbiased. It is not trivial, however, to generalize (A5) to unequal masses.

In the text, R_v was estimated from (A1) for models with $F_b = 0$, and (A4) for the others V_v was always estimated from (A2), using the fact that $\bar{\mathbf{V}} \equiv 0$ in the frame of the N-body calculation [observers, who must estimate $\bar{\mathbf{V}}$, may be better off using (A5)]. In practice, the uncertainties due to the choice of estimator were usually small.